[1]N.Eguchi [2]K.Kodera [3]T.Nasuno
pdftitle=Downward coupling in the TTL
pdfauthor=N. Eguchi et al.
title Manuscript prepared for Atmos. Chem. Phys. Discuss.
with version 4.1 of the LaTeX class copernicus_discussions.cls.
Date: 10 November 2014

A global non-hydrostatic model study of a downward coupling through the tropical tropopause layer during a stratospheric sudden warming

Research Institute for Applied Mechanics, Kyushu University, Kasuga, Japan

Solar-Terrestrial Environment Laboratory, Nagoya University, Nagoya, Japan

Research Institute for Global Change, Japan Agency for Marine-Earth Science and Technology, Yokohama, Japan

Correspondence to: N. Eguchi (nawo@riam.kyushu-u.ac.jp)

Abstract

The dynamical coupling process between the stratosphere and troposphere in the tropical tropopause layer (TTL) during a stratospheric sudden warming (SSW) in boreal winter was investigated using simulation data from a global non-hydrostatic model (NICAM) that does not use cumulus parameterization. The model reproduced well the observed tropical tropospheric changes during the SSW including the enhancement of convective activity following the amplification of planetary waves. Deep convective activity was enhanced in the latitude zone 20–10° S, in particular over the southwest Pacific and southwest Indian Ocean. Although the upwelling in the TTL was correlated with that in the stratosphere, the temperature tendency in the TTL changed little due to a compensation by diabatic heating originating from cloud formation. This result suggests that the stratospheric meridional circulation affects cloud formation in the TTL.

1 Introduction

There have been many studies on the interaction between the stratosphere and troposphere in the tropical tropopause layer (hereafter, TTL), which is typically located at 14–19 km altitude or 150–90 hPa (Highwood and Hoskins, 1998; Fueglistaler et al., 2009), with stratospheric water vapor variation on interannual and seasonal time scales (cf., Randel and Jensen, 2013) an important topic. Possible impacts of the recent stratospheric cooling trend on the troposphere, such as an increase of intensity in tropical cyclones, are currently the subject of discussion (Emanuel et al., 2013; Ramsay, 2013). However, it is difficult to separate the stratospheric effect on the troposphere from other factors for long-term variations such as a warming of the ocean.

Here, we focus on changes in the troposphere, especially in the TTL, during a stratospheric sudden warming (hereafter, SSW) event, which drastically modifies the stratospheric circulation (Brewer–Dobson (BD) circulation) in the space of a week, because the tropical convection and the general circulation (the Hadley and Walkerwere cells) rapidly changed during the strong SSW events found by some previous observational studies (e.g., Eguchi and Kodera, 2007, 2010 (EK10)). Further, because of the short duration phenomenon, the impact of SSW on the tropical

troposphere can be separated from long-term variability such as the Madden–Julian Oscillation (MJO), El Nino–Southern Oscillation (ENSO), or the Quasi-Biennial Oscillation (QBO). However, it is still not clear how the connection between the stratosphere and troposphere occurs and how it modulates the convective activity during SSW events.

This is largely due to a lack of global observations of vertical velocity in the TTL. Ueyama et al. (2013) showed that the temperature tendency in the stratosphere can be used as a proxy for the vertical motion (i.e., the strength of BD circulation). However, this relationship does not hold below the tropopause, where diabatic heating due to cloud formation cancels adiabatic cooling, as will be shown later.

Data from numerical simulation are useful for examining vertical velocity in the TTL. Thuburn and Craig (2000) used momentum forcing in a simplified global general circulation model (GCM) to show that a change in the stratospheric meridional circulation modified cumulus heating in the TTL as well as the tropopause height. Kodera et al. (2011) constructed a more realistic forecast experiment by incorporating an atmospheric blocking-type circulation anomaly in the North Atlantic in the initial conditions to amplify planetary waves and produce strong BD circulation later in the stratosphere. The results showed similar effects in the tropics to those seen in observational studies, that is, the tropical convective activity was enhanced zonally, especially in the Southern Hemisphere (SH), and cooling at the tropopause region associated with the SSW event was capable of modulating tropical convective activity.

These results suggest that convection plays an important role in the stratosphere–troposphere coupling in the tropics. In these models, however, the effects of convection were not explicitly treated, but were represented by cumulus parameterization. Thus, dependence on the parameterization was unavoidable. Furthermore, examination of thermodynamic processes in the TTL using the higher resolution GCM is desired to clarify the coupling process between the stratosphere and troposphere, where the thermo–dynamic balance is complicated. In the present study, convective change during a SSW event that occurred in January 2010 is investigated using a high-resolution global simulation data from a global non-hydrostatic model, NICAM (non-hydrostatic icosahedral atmospheric model) (Satoh et al., 2008, 2014), in which a cumulus parameterization was not employed. This allows discussion of the dynamic and thermodynamic

changes in the TTL without any prescribed relationship between dynamics and moist convection. A case study using such high-resolution simulation data has the advantage of capturing the fine vertical and temporal structures of the TTL during the SSW event, which might be smoothed away in a statistical analysis of a huge number of events occurring under a range of conditions.

The remainder of the paper is organized as follows. The next section deals with the NICAM simulation data (Sect. 2), Sect. 3 shows the SSW event simulated in NICAM and the dynamical variability in the stratosphere and troposphere during the SSW. A summary and discussion of the results are given in Sect. 4.

2 Analysis data

The numerical simulation was conducted using NICAM, the global non-hydrostatic model with a horizontal mesh size of 14 km and 40 vertical levels. Kodama et al. (2012) assessed cloud signals in NICAM simulations and demonstrated that the gross behaviors of clouds can be statistically reproduced with 14 km mesh size, although individual clouds are not sufficiently resolved. The main purpose of the present study is not a realistic presentation of an individual cloud, but investigation of diabatic heating processes in the TTL without any prescribed relationship between convection and dynamics as assumed in a cumulus parameterization. The use of 14 km horizontal mesh size and 38 km model top is marginal to a TTL study, which will be followed by numerical studies with more suitable setups (Satoh et al. 2014). Nevertheless, the BD circulation and the seed of the SSW events included in the initial data, which was interpolated from an objective analysis, led to spontaneous occurrences of reasonable atmospheric circulation and convection in the model for the simulation period, as shown in Section 3.

The model top was at 38 km with nine layers between 10 km and 20 km altitude. The impact of low model top on the planetary wave propagation has been studied. If model top is simply lowered, large difference occurs in the troposphere as well as in the stratosphere. However, if some readjustment of the wave dissipation is made, lower stratospheric circulation becomes

more or less realistic (Boville and Chen, 1988). Present study mainly concerns circulation lower than about 25 km, so that NICAM model of which model top at 38 km can be used.

Moist convection was explicitly calculated using a cloud microphysical scheme (single moment scheme) with six prognostic variables (Tomita, 2008). Atmospheric radiation, turbulence, and ocean processes were calculated using the MSTRN-X (Nakajima et al., 2000; Sekiguchi and Nakajima, 2008), Mellor–Yamada–Nakanishi–Niino level 2 (Mellor and Yamada, 1982; Nakanishi and Niino, 2006; Noda et al., 2010), and slab ocean models, respectively. The sea surface temperature (SST) was initialized using the National Centers for Environmental Prediction (NCEP) final (FNL) operational global analysis data ($1^\circ \times 1^\circ$), and nudged to the NOAA weekly Optimum Interpolation SST analysis (Reynolds and Smith, 1994) with a relaxation time of seven days.

The atmospheric initial data were interpolated from the ECMWF YOTC (Year of tropical Convection) analysis (Waliser et al., 2012). The simulation period was the 60 days starting from 20 December 2009. During this period, a significant MJO event took place (Waliser et al., 2012), and this MJO event was targeted in a model intercomparison project (http://yotc.ucar.edu/mjo/vertical-structure-and-diabatic-processes-mjo). The cloud properties in the upper troposphere (UT) have been evaluated in comparison with satellite observations (e.g., Inoue et al., 2010; Kodama et al., 2012).

In the present study, winds (zonal, meridional and vertical), temperature, specific humidity, diabatic heating rates (by cloud microphysics and solar radiation), snow, ice and graupel contents, and column integrated cloud fraction were analyzed. The cloud fraction data are two-dimensional (longitude–latitude), and the others are three-dimensional. Snapshot data were archived at 3 h intervals except for cloud fraction (hourly mean) and diabatic heating rate (daily mean). All the output variables were daily averaged and converted into 1° datasets.

3 Results

3.1 Stratospheric sudden warming simulated by NICAM

In the real atmosphere, the SSW in the boreal hemisphere occurred during January 2010 (cf., Dörnbrack et al., 2012). The temperature increased by $+35\,\mathrm{K}$ in the northern polar region and decreased by $-2.5\,\mathrm{K}$ in the tropical lower stratosphere (LS) with increasing wave activity at middle latitudes (Fig. 1a and b). In the NICAM simulation, minor stratospheric warming spontaneously occurred in January 2010, although the date on which the tropical lower stratospheric (approximately 50–80 hPa) temperature started decreasing was approximately five days earlier than in the real atmosphere. The temperature rose in the polar region, but decreased in the tropics (Fig. 2a) because enhanced wave activity at middle latitudes (Fig. 4c) induced downwelling in the polar region and upwelling in the tropics in the stratosphere. The temperature variation was comparable to that in the real atmosphere: the temperature rose by approximately $+25\,\mathrm{K}$ in the northern polar region and fell $-1.5\,\mathrm{K}$ in the tropics after 7 January.

The tropical averaged temperature in the LS decreased gradually from 14 January; the latitude–time section of the LS temperature (Fig. 2b) shows that cooling on the south side of the equator starts around 14 January before that on the north side. In the tropical troposphere, the center of the region of active convection shifted southward from 5° S to 15° S after 14 January, when the LS started cooling. The latitude of minimum temperature (Fig. 2b) was located to the south of the convective region (around 25° S; Fig. 2c), here the LS upwelling was enhanced in period (ii).

After 21 January, cooling occurred over the wide tropics (30° S–30° N) with an equatorially symmetric structure (Fig. 2b). The largest column integrated cloud fraction occurred in association with the cooling in the tropical LS around 24 January. Note that the column integrated cloud fraction includes both convective and upper level thin clouds. The convective clouds are measured by outgoing longwave radiation (OLR). The region of minimum OLR shifted southward from 5°S to 12.5°S after 14 January. The upper level clouds (ice clouds) shifted also southward and extended farther southward (15°S) compared to convective clouds (Fig. 2d). In the real atmosphere, the convective region was shifted southward around 20 January and en-

hanced around 2 February (Fig. 1c). The convective initiation of the MJO event took place over the western Indian Ocean at the end of December 2009, and the MJO propagated eastward during January 2010. The SSW occurred when the MJO passed over the maritime continent. In the simulation, the MJO was weaker than in the observations,the eastward propagation started at the end of period (ii) or the beginning of the period (iii) (figure is not shown). Further, the equatorial convection in the simulation (also observation) was suppressed during the period (ii) (when convection was passing over the maritime continent in the observation), because the convective activity regions shifted southward off equatorial southern hemisphere. It is suggested that the convection behavior cannot be explained only by eastward travelling convective signal, such as MJO. Thus, the effects of the MJO are expected to be small for the simulated convective variations during the target two weeks.

We divided the period into three consecutive seven-day periods according to the LS tropical temperature (Fig. 2): period (i) (7–13 January) is prior to the start of the cooling event. Period (ii) (14–20 January) is characterized by a cooling trend, while period (iii) (21–27 January) is the period of peak cooling. These periods could be regarded as the initiation, transition, and mature phases of the SSW impact on the tropics, respectively.

3.2 Connection between stratospheric and tropospheric meridional circulation

Ueyama et al. (2013) demonstrated that the tropical temperature tendency at 70 hPa (LS) is closely related to the strength of the stratospheric meridional circulation. To investigate in more detail the structure of the coupling between the stratospheric and tropospheric circulation, the temporal correlation coefficient between the tropical mean vertical velocity at 70 hPa and the zonal mean vertical velocity at each level was calculated (Fig. 3a). The vertical velocity at 100 hPa (TTL) was not correlated with that at 70 hPa, except near 20° S. However, better correlation is found in the deep troposphere and the LS in a latitudinal zone of 20° S–10° S where the convection is enhanced in period (ii) as shown in Fig. 2c. These features are also confirmed in time-longitude sections (not shown).

Variation of the vertical velocity in the troposphere usually accompanies a change in cloud formation. The difference in diabatic heating due to cloud microphysics between periods (ii)

and (i) is displayed in Fig. 3b. A large change in the diabatic heating is found between 20–10° S corresponding to the zone of enhanced upwelling from the surface to the TTL. In the TTL (at 100 hPa), an increase of the diabatic heating extended all over the tropics including the Northern Hemisphere (NH). This zone of increased diabatic heating just below 70 hPa corresponds to a zone of decreased water vapor (Fig. 3c), as upwelling induces adiabatic cooling leading to sublimation of water vapor. The cooling trend in the TTL was evident over the wide tropics (Fig.2b).

Cirrus cloud forms in the TTL (30° S–20° N) after the onset of the SSW, although higher correlations of vertical wind with that over the tropical LS are limited to within the convective region (20–10° S). In other words, the low correlation between the vertical motion in the LS and that in the TTL (around 100 hPa) implies that the mechanisms of the formation of ice clouds in the TTL were different from those of convective clouds in the tropical deep troposphere. The next subsection will describe the detailed mechanism of ice cloud formation in the TTL.

Figure 3b and c also shows that the increased diabatic heating in the deep troposphere occurs in association with an increase of water vapor in the lower troposphere. This is indicative of positive feedback between convective activity and low-level moisture convergence in the lower troposphere (EK10) over the tropical SH in period (iii) as illustrated in Fig. 2c.

3.3 Downward propagation of dynamical signal through the TTL

Time–altitude sections of the temperature tendency, static stability and anomalous vertical velocity are displayed in Fig. 4. The static stability is defined by $\frac{g}{\theta}\frac{\partial\theta}{\partial z}$, where g is the acceleration due to gravity ($9.81\,\mathrm{ms}^{-2}$) and θ is potential temperature [K]. Variables are averaged over the tropical band between 20° S and Equator, where the convective activity and the upwelling in the TTL showed clear changes during the SSW event (Fig. 3).

Temperatures started decreasing in the LS and the upper TTL (above 17.5 km) around 15 January, but increased in the troposphere. The region of weak negative temperature trend then propagated downward in the TTL during period (ii) and (iii). The zone of weaker static stability also descended through the TTL following the negative temperature trend. The anomalous vertical velocity (Fig. 4b) showed a strengthening of the upwelling propagating from the LS to the

UT in period (ii), similar to the temperature tendency, but with enhancement in the deep troposphere during period (iii), when total column integrated cloud fraction was the largest (Fig. 2c).

To understand the different characteristics of the variations in temperature tendency and vertical velocity, we investigated the major terms (the term on the LHS and first two terms on the RHS of the following equation) of the thermodynamic equation in the Transformed Eulerian Mean (TEM) framework (Andrews et al., 1987);

$$\overline{\frac{\partial T}{\partial t}} = -N^2\overline{w^*}\left(\frac{\overline{P_0}}{P}\right)^{-\kappa} + \overline{\mathrm{DH}} - \frac{\overline{v^*}}{a}\overline{\frac{\partial T}{\partial \phi}} - \frac{1}{\rho_0}\frac{\partial}{\partial z}\left[\rho_0\left(\frac{\overline{v'T'}}{a\,\overline{\frac{\partial T}{\partial z}}}\overline{\frac{\partial T}{\partial \phi}} + \overline{w'T'}\right)\right].$$

Here T is temperature, N is Brunt–Väisälä frequency, w^* (v^*) is the vertical (meridional) component of residual velocity, DH is diabatic heating rate (cloud microphysics and radiation), $P(P_0)$ is (reference) pressure and κ is R/C_p (0.286), (where R is the gas constant and C_p is the specific heat at constant pressure). The third and fourth terms of the RHS of the equation are meridional advection and diffusion by waves and eddies, respectively.

The temperature tendency agrees quite well with the adiabatic cooling rate at 20 km (LS) (Fig. 4d). The evolution of these curves matches that of the eddy heat flux ($\overline{v'T'}$) at 100 hPa averaged over the extratropical NH (Fig. 4c). Note also that the radiative diabatic heating rate remains almost constant at $+0.5 \sim 0.6\,\mathrm{K\,day^{-1}}$, which balance the third and fourth terms on the RHS of the above thermodynamic equation.

At the bottom part of the TTL (14.3 km in Fig. 4e), the adiabatic and diabatic heating were almost in balance, while the adiabatic cooling associated with the stratospheric upwelling drove the temperature tendency at greater heights (above 14.3 km). Meanwhile, the heat balance in the TTL was also related to the longitudinal distributions of diabatic heating due to cloud microphysics and solar (shortwave) radiation.

Figure 5a and b shows the horizontal variation of the latent heating rate due to cloud microphysics as an indicator of cloud formation at the bottom of the TTL (14.3 km). Figure 5c and d shows the longitude–height section of vertical velocity averaged over 20° S–Equator. Left and right panels display the averages during periods (i) and (ii), respectively. In period (i), before the SSW event started, clouds formed mainly along the intertropical convergence zone (ITCZ)

and over the southwestern Pacific region in the UT, which extended up to the TTL. In the TTL, clouds were also found over equatorial Africa and South America.

When the LS in the southern tropics started to cool in period (ii), convective activity in the TTL shifted southward and increased along the latitudes 20–10° S (Fig. 3b), particularly over the southwestern Pacific, southwestern Indian Ocean, and coastal regions of South America. The development of convective intensity and depth from the period (i) to (ii) is apparent in the pressure–longitude section of vertical velocity, especially over the western Pacific and the western Indian Ocean (Fig. 5c and d). The upward motion above the TTL, especially at 85 hPa, became dominant in period (ii).

Thus, diabatic heating and vertical motion associated with deep convection with zonally asymmetric distributions influenced the heat balance in the UT and TTL, whereas in the LS the effects of zonally symmetric vertical motion were dominant (as indicated by Figs. 4d, e and 5c, d).

4 Summary and discussion

The present study investigates stratospheric dynamical impacts on the tropical tropospheric convection during a SSW event from the view point of thermo-dynamic balance in the TTL. As a pilot study, simulation data from a global non-hydrostatic model (NICAM), where moist convection is explicitly represented, was analyzed. The impact of the SSWs has been confirmed in a previous ensemble mean forecast study of a conventional GCM, by implementing a perturbation in the extratropical initial field to produce or to suppress the SSW (Kodera et al., 2011). Note, however, that the cumulus convection is parameterized in this GCM, so that we further needs to verify whether the similar results are obtained by using a global cloud resolving model. The model reproduced the observed processes during SSW: convective activity in the tropical SH was enhanced following an amplification of extratropical planetary wave activity in the winter NH. Vertical velocity and diabatic heating, which are difficult to observe, are intensively investigated.

The stratosphere–troposphere connection was detected in the correlation coefficient between the tropical stratospheric upwelling and the vertical velocity in the tropical troposphere. The highest correlation was found in the SH 20–10° S latitudinal band (Fig. 3a), where the upwelling branch of BD circulation in the summer hemisphere is located for this case. Particularly large variation is found over in Fig.5 over the southwestern Indian Ocean, southwestern Pacific and coastal region of Australia similar to the observation (Fig.3 in Kodera et al., 2014).

Although upwelling in the troposphere occurs following that of the stratosphere, they were not produced by the same process (Fig. 4). Vertical velocity over the wide tropics (e.g. 30° S–30° N) in the LS is mainly driven by extratropical planetary waves (Ueyama et al., 2013; Abalos et al., 2013), but that in the UT was affected mainly by deep convection in a more restricted zone around 20° S–10° S.

Impact of increased stratospheric upwelling can be seen one as decrease of water vapor around the tropical tropopause region, and the other is increase of water vapor around upwelling branch of the Hadley cell in summer hemisphere (15°S) (Fig. 3b). The former effect around the tropopause is due to a condensation of water vapor by large scale cooling associated with enhanced tropical upwelling in the lower stratosphere (Li and Thompson, 2013). The other effect can be attributed to an increased overshooting and deep convective activity due to decreased static stability in the TTL as a consequence of adiabatic cooling in the lower stratosphere and diabatic heating in the TTL (Fig. 4).

This impact of decreased stability on the convective activity was studied by Chae and Sherwood (2010) with a non-hydrostatic regional model of 28 $\times$ 600 km domain. Similar effect is confirmed for the present case. Moreover, the global model also showed the occurrences of more complex processes: large scale organization of convective activity and the associated decrease of water vapor in the tropical NH (Fig. 3). The large scale change in convection took place as mesoscale organization of convective system, such as tropical cyclone or storms (Fig. 5), which can also be found in observational results (Kodera et al., 2014). To clarify such complex processes, we further needs specific numerical experiments, by using an updated version of the global non-hydrostatic model.

There is uncertainty in the present results because of single simulation analysis. To clarify further the causal relationship between the tropical troposphere change and the stratospheric circulation change, in the near future work, the statistical analysis by using the longer simulation and/or the comparison study by the simulations with/without SSW will be helpful.

Acknowledgements. The NICAM simulation was performed on the Earth Simulator. The authors would like to thank Chihiro Kodama at the Japan Agency for Marine-Earth Science and Technology (JAMSTEC) for his useful comments. This study was supported by JSPS KAKENHI Grant-in-Aid for Young Scientists (B), number 23710025 and JSPS KAKENHI Grant-in-Aid for Scientific Research (C), number 25340010.

References

Abalos, M., W.J. Randel and E. Serrano : Dynamical forcing of sub-seasonal variability in the tropical Brewer-Dobson circulation, J. Atmos. Sci., in press.

Andrews, D. G., Holton, J. R., and Leovy, C. B.: Middle Atmosphere Dynamics, Academic Press, Orlando, Florida, 489 pp., 1987.

Boville, Byron A. and Xinhua Cheng, Upper Boundary Effects in a General Circulation Model. J. Atmos. Sci., 45,2591–2606, 1988.

Chae, J-H and S. C. Sherwood, Insights into cloud-top height and dynamics from the seasonal cycle of cloud-top heights observed by MISR in the West Pacific region. J. Atmos. Sci., 67, 248–261, 2010.

Dörnbrack, A., Pitts, M. C., Poole, L. R., Orsolini, Y. J., Nishii, K., and Nakamura, H.: The 2009–2010 Arctic stratospheric winter – general evolution, mountain waves and predictability of an operational weather forecast model, Atmos. Chem. Phys., 12, 3659–3675, doi:http://dx.doi.org/10.5194/acp-12-3659-201210.5194/acp-12-3659-2012, 2012.

Eguchi, N. and Kodera, K.: Impact of the 2002, Southern Hemisphere, stratospheric warming on the tropical cirrus clouds and convective activity, Geophys. Res. Lett., 34, L05819, doi:http://dx.doi.org/10.1029/2006GL02874410.1029/2006GL028744, 2007.

Eguchi, N. and Kodera, K.: Impacts of stratospheric sudden warming event on tropical clouds and moisture fields in the TTL: a case study, SOLA, 6, 137–140, doi:http://dx.doi.org/10.2151/sola.2010-03510.2151/sola.2010-035, 2010.

Emanuel, K., Solomon, S., Folini, D., Davis, S., and Cagnazzo, C.: Influence of tropical tropopause layer cooling on Atlantic hurricane activity, J. Climate, 26, 2288–2301, 2013.

Fueglistaler, S., Dessler, A. E., Dunkerton, T. J., Folkins, I., Fu, Q., and Mote, P. W.: Tropical tropopause layer, Rev. Geophys., RG1004, doi:http://dx.doi.org/10.1029/2008RG00026710.1029/2008RG000267, 2009.

Highwood, E. J. and Hoskins, B. J.: The tropical tropopause, Q. J. Roy. Meteor. Soc., 124, 1579–1604, 1998.

Inoue, T., Satoh, M., Hagihara, Y., Miura, H., and Shmetz, J.: Comparison of high-level clouds represented in a global cloud system-resolving model with CALIPSO/CloudSat and geostationary satellite observations, J. Geophys. Res.-Atmos., 115, D00H22, doi:http://dx.doi.org/10.1029/2009JD01237110.1029/2009JD012371, 2010.

Kodama, C., Noda, A. T., and Satoh, M.: An assessment of the cloud signals simulated by NICAM using ISCCP, CALIPSO, and CloudSat satellite simulators, J. Geophys. Res.-Atmos., 117, D12210, doi:http://dx.doi.org/10.1029/2011JD01731710.1029/2011JD017317, 2012.

Kodera, K., B. M. Funatsu, C. Claud, and N. Eguchi, The role of convective overshooting clouds in tropical stratosphere–troposphere dynamical coupling, Atmos. Chem. Phys. Discuss., 14, 23745-23761, 2014.

Kodera, K., Mukougawa, H., and Kuroda, Y.: A general circulation model study of the impact of a stratospheric sudden warming event on tropical convection, SOLA, 7, 197–200, doi:http://dx.doi.org/10.2151/sola.2011-05010.2151/sola.2011-050, 2011.

Li, Y. and Thompson, D. W. J.: The signature of the stratospheric Brewer–Dobson circulation in tropospheric clouds, J. Geophys. Res.-Atmos., 118, 3486–3494, doi:http://dx.doi.org/10.1002/jgrd.5033910.1002/jgrd.50339, 2013.

Mellor, G. L. and Yamada, T.: Development of a turbulent closure model for geophysical fluid problems, Rev. Geophys., 20, 851–875, 1982.

Nakajima, T., Tsukamoto, M., Tsushima, Y., Numaguti, A., and Kimura, T.: Modeling of the radiative process in an atmospheric general circulation model, Appl. Optics, 39, 4869–4878, doi:http://dx.doi.org/10.1364/AO.39.00486910.1364/AO.39.004869, 2000.

Nakanishi, M. and Niino, H.: An improved Mellor–Yamada level-3 model: its numerical stability and application to a regional prediction of advection fog, Bound.-Lay. Meteorol., 119, 397–407, 2006.

Noda, A. T., Oouchi, K., Satoh, M., Tomita, H., Iga, S., and Tsushima, Y.: Importance of the subgrid-scale turbulent moist process: cloud distribution in global cloud-resolving simulations, Atmos. Res.,

96, 208–217, doi:http://dx.doi.org/10.1016/j.atmosres.2009.05.00710.1016/j.atmosres.2009.05.007, 2010.

Ramsay, H. A.: The effects of imposed stratospheric cooling on the maximum intensity of tropical cyclones in axisymmetric radiative–convective equilibrium, J. Climate, 26, 9977–9985, doi:http://dx.doi.org/10.1175/JCLI-D-13-00195.110.1175/JCLI-D-13-00195.1, 2013.

Randel, W. J. and Jensen, E. J.: Physical processes in the tropical tropopause layer and their role in a changing climate. Nat. Geosci., 6, 169–176, doi:http://dx.doi.org/10.1038/ngeo173310.1038/ngeo1733, 2013.

Reynolds, R. W. and Smith, T. M.: Improved global sea surface temperature analyses using optimum interpolation, J. Climate, 7, 929–948, 1994.

Satoh, M., Matsuno, T., Tomita, H., Miura, H., Nasuno, T., and Iga, S.: Nonhydrostatic icosahedral atmospheric model (NICAM) for global cloud resolving simulations, J. Comput. Phys., 227, 3486–3514 doi:http://dx.doi.org/10.1016/j.jcp.2007.02.00610.1016/j.jcp.2007.02.006, 2008.

Satoh, M., H. Tomita, H. Yashiro, H. Miura, C. Kodama, T. Seiki, A. T. Noda, Y. Yamada, D. Goto, M. Sawada, T. Miyoshi, Y. Niwa, M. Hara, T. Ohno, S. Iga, T. Arakawa, T. Inoue, H. Kubokawa, 2014: The Non-hydrostatic Icosahedral Atmospheric Model: description and development. Prog. Earth Planet. Sci., 1, 18. doi:http://dx.doi.org/10.1186/s40645-014-0018-110.1186/s40645-014-0018-1, 2014.

Sekiguchi, M. and Nakajima, T.: A k-distribution-based radiation code and its computational optimization for an atmospheric general circulation model, J. Quant. Spectrosc. Ra., 109, 2779–2793, 2008.

Thuburn, J. and Craig, G. C.: Stratospheric influence on tropopause height: the radiative constraint, J. Atmos. Sci., 57, 17–28, doi:10.1175/1520-0469(2000)057–0017:SIOTHT–2.0, 2000.

Tomita, H.: New micorphysical schemes with five and six categories by diagnostic generation of cloud ice, J. Meteorol. Soc. Jpn., 86A, 121–142, 2008.

Ueyama, R., Gerber, E. P., Wallace, J. M., and Frierson, D. M. W.: The role of high-latitude waves in the intraseasonal to seasonal variability of tropical upwelling in the Brewer–Dobson circulation, J. Atmos. Sci., 70, 1631–1648, doi:http://dx.doi.org/10.1175/JAS-D-12-0174.110.1175/JAS-D-12-0174.1, 2013.

Waliser, D. E., Moncrieff, M., Burridge, D., Fink, A. H., Gochis, D., Goswami, B. N., Guan, B., Harr, P., Heming, J., Hsu, H.-H., Jakob, C., Janiga, M., Johnson, R., Jones, S., Knippertz, P., Marengo, L., Nguyen, H., Pope, M., Serra, Y., Thorncroft, C., Wheeler, M., Wood. R., and Yuter, S.: The "Year" of tropical convection (May 2008–April 2010): climate variability and weather highlights. B. Am. Meteorol. Soc., 93, 1189–1218, 2012.

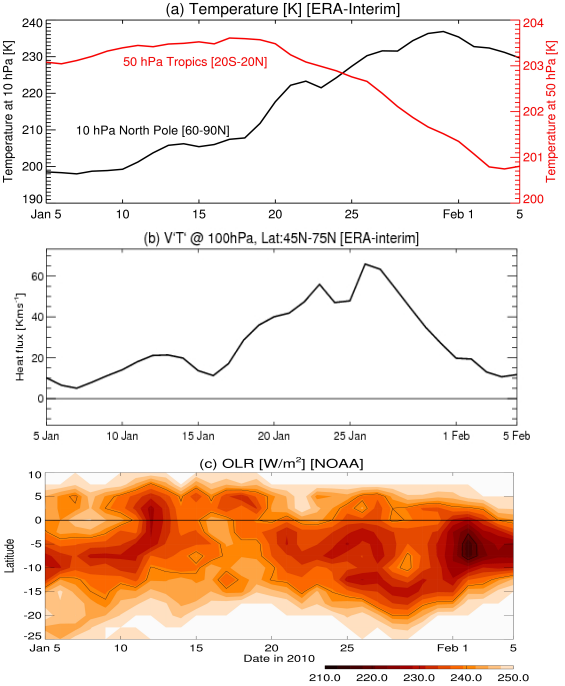

Fig. 1. (a) Time series of observed zonal mean temperature [K] in the northern high latitude at 10 hPa (black line) and tropical at 50 hPa (red line) from 5 January to 5 February, 2010. Note the different temperature scales for the polar (left) and tropical (right) regions. **(b)** Time series of observed zonal mean eddy heat flux [$\mathrm{K\,m\,s^{-1}}$] at 100 hPa averaged between 45° N and 75° N. **(c)** Time–latitude (25° S–10° N) section of NOAA observed zonal mean OLR [$\mathrm{W\,m^{-2}}$]. The horizontal line indicates the equator. figure

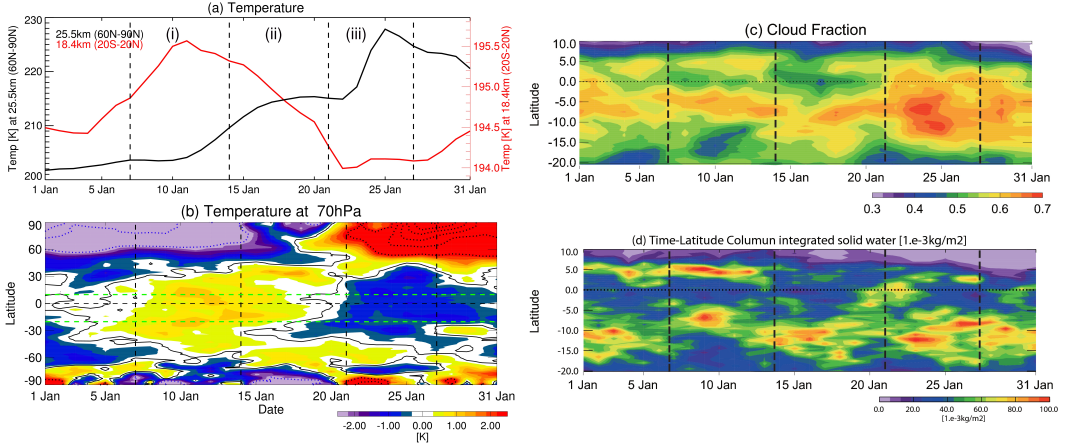

Fig. 2. **(a)** Same as Fig. 1a but for simulated zonal mean temperature from 1 to 31 January 2010. **(b)** Time–latitude (90° N–90° S) section of simulated temperature anomaly [K] at 70 hPa with respect to the January 2010 monthly mean at each latitude. The solid contour indicates zero anomaly and the dotted contours indicate −2.5 K and 2.5 K. The light green horizontal dashed lines indicate the latitudinal region of **(c) and d**. **(c)** Time–latitude (20° S–10° N) section of simulated zonal mean column integrated cloud fraction. **(d)** Same as **(c)** but for column integrated ice cloud $[10^{-3}\ kg\ m^{-2}]$. The four vertical dashed lines in **(a–d)** are 7, 14, 21 and 27 January; the periods between the lines are the (i) initial, (ii) transition and (iii) mature phases, respectively. The horizontal dashed lines in (**b**, **c** and **d**) indicate the equator.

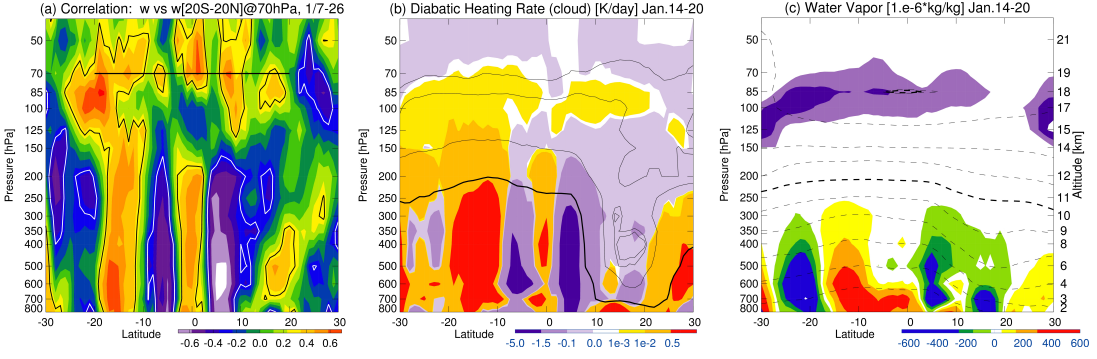

Fig. 3. (a) Latitude–pressure sections of correlation between the vertical wind averaged over 20° S–20° N at 70 hPa (thick line) and vertical wind at each level and latitude for the period of 7–26 January. Latitude–pressure sections of **(b)** latent heating rate due to cloud formation $[\mathrm{K\,day^{-1}}]$ (contours) and **(c)** the water vapor concentration $[10^{-6}\,\mathrm{kg\,kg^{-1}}]$ (dashed contours) averaged between 14 and 20 January. The thin contours in **(b)** are values of $10^{-3}\times 10^{i}$ $(i=0,1,2)$ $[\mathrm{K\,day^{-1}}]$. The thick contour is 1.0 $[\mathrm{K\,day^{-1}}]$. The dashed contours in **(c)** are values of $10^{4}\times 10^{i/3}$ $(i=0,1,2,\ldots,10)$ $[10^{-6}\,\mathrm{kg\,kg^{-1}}]$; the thick dashed contours indicate 4.6 and 100 $[10^{-6}\,\mathrm{kg\,kg^{-1}}]$. Anomalies with respect to the 7–13 January average are shown by color shading. The light and heavy purple in **(c)** indicate values of -0.3 $[10^{-6}\,\mathrm{kg\,kg^{-1}}]$ and below, -0.6 $[10^{-6}\,\mathrm{kg\,kg^{-1}}]$ and below.

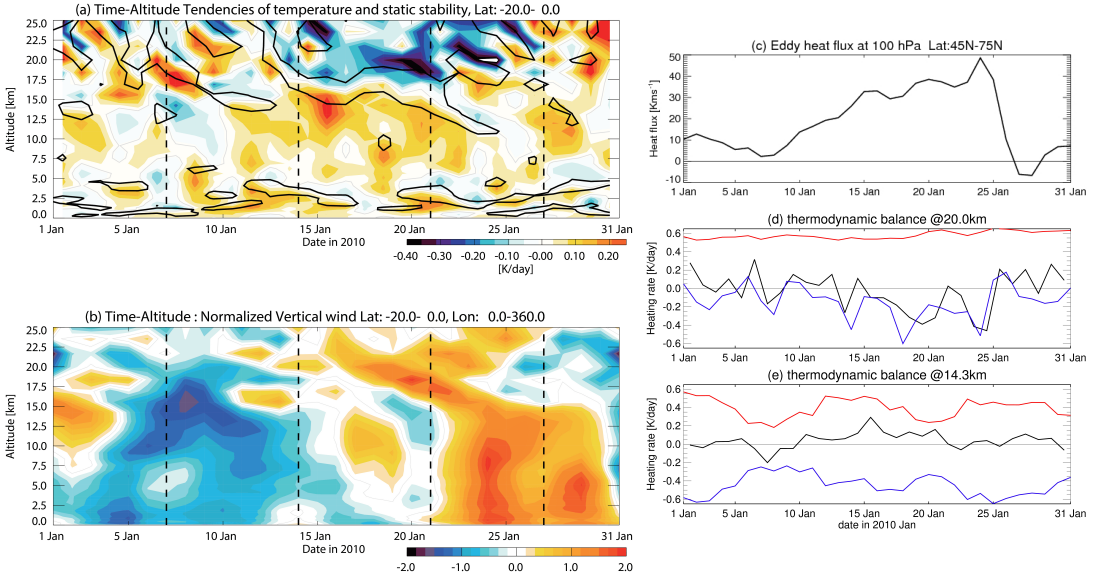

Fig. 4. Time–altitude section of **(a)** temperature tendency $[\mathrm{K\,day^{-1}}]$ (color shading) and tendency of static stability with value of -0.02 $[10^{-4}\,\mathrm{s^{-2}\,day^{-1}}]$ shown by black contours, and **(b)** anomalous normalized vertical velocity averaged between 20° S and Equator from 1 to 31 January 2010. The normalized values are obtained by dividing by the standard deviation at each altitude. **(c)** Time series of zonal mean eddy heat flux $[\mathrm{K\,m\,s^{-1}}]$ at 100 hPa averaged between 45° N and 75° N. **(d, e)** show the time series of thermodynamic balance at 14.3 and 20.0 km averaged between 20° S and Equator. The black, red and blue lines indicate temperature tendency ($\partial T/\partial t$), diabatic heating rate due to cloud microphysics and radiation, and adiabatic heating rate due to residual vertical velocity ($-N^2\omega^*$), respectively.

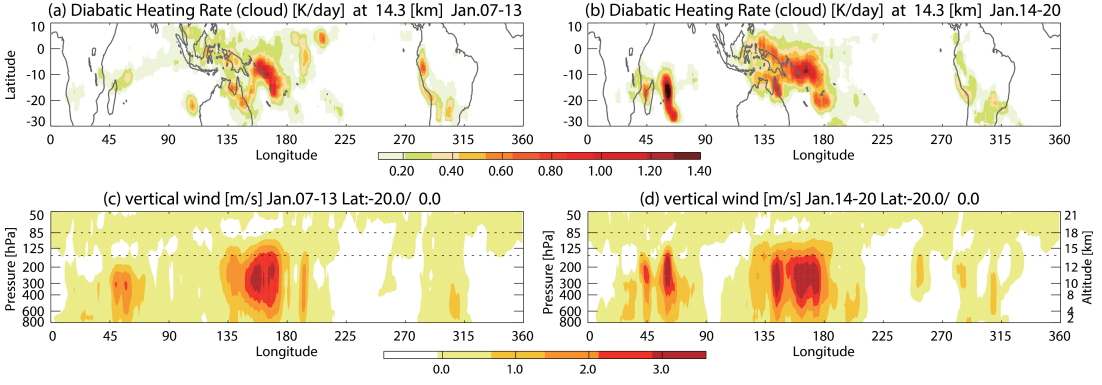

Fig. 5. Maps of diabatic heating rate from cloud microphysics [$\mathrm{K\,day^{-1}}$] at 14.3 km **(a, b)** averaged over 7–13 January (left, **a**) and 14–20 January (right, **b**). The panels **(c, d)** show longitude–pressure sections of vertical wind [$\mathrm{m\,s^{-1}}$] averaged between 20° S and Equator on 7–13 and 14–20 January, respectively. The vertical wind data are smoothed by applying a weighting function of five-degree-longitude width. The horizontal dotted lines in **(c, d)** show the 85 hPa and 150 hPa pressure levels for reference.